Chapter 7

Soil Contamination Mapping with Hyperspectral Imagery: Pre-Dnieper Chemical Plant (Ukraine) Case Study

Sergey A. Stankevich, Mykola M. Kharytonov,
Anna A. Kozlova, Vadym Yu. Korovin,
Mykhailo O. Svidenyuk and Alexander M. Valyaev

Additional information is available at the end of the chapter

http://dx.doi.org/10.5772/intechopen.72601

Abstract

Radioactive contamination of soils is an issue of severe importance for Ukraine remaining with a significant post-Soviet baggage of not settled problems regarding radioactive waste. Regular radioecological observations and up-to-date contamination mapping based on advanced geoinformation techniques give an ability to prepare for, respond to, and manage potential adverse effects from pollution with radionuclides and heavy metals. Hyperspectral satellite imagery provides potentially powerful tool for soil contamination detection and mapping. An intention to find a relation between remotely sensed hyperspectral and ground-based measured soil contamination fractions in area of the uranium mill tailings deposits near Kamianske city was made. An advanced algorithm based on known TCMI (target-constrained minimal interference)-matched filter with a nonnegative constraint was applied to determine the soil contamination fractions by hyperspectral imagery. The time series maps of spatial distribution of the soil contamination fractions within study area around the Sukhachevske tailings dump are presented. Time series analysis of the map resulted in two independent parameters: the average value for the entire observation period and the daily mean increment of the soil contamination fractions.

Keywords: Pre-Dnieper chemical plant, uranium mill tailings, soil contamination fractions, hyperspectral imaging, spectral unmixing, time series analysis

1. Introduction

Nowadays, agriculture became the leading branch of the Ukrainian economy. Ukraine places among the world's top 10 producers of wheat, barley, corn, and soybeans and is the leader

in the production and export of sunflower. One-third of Ukrainian agrarian products are exported to European countries. Such agricultural achievements are primarily caused by the rich land potential of the country. There are 60.4 million hectares of mollisols in Ukraine. Moreover, almost 42 million hectares (about 69%) of them are arable lands and farmlands. The southern and central regions of Ukraine are especially fertile due to the highest content of humus in the local mollisols [1].

According to the Constitution of Ukraine, "Land shall be the main national asset and as such shall be under special protection" (Art. 14). Nevertheless, more than half of the fertile lands in Ukraine suffer from different types of degradation: loss of the fertile layer, erosion, and contamination. The problem of radioactive contamination of soils is extremely topical for Ukraine [2].

The mining and processing of uranium ore started in Soviet Ukraine in the late 1940s as a secret without any requirements of environmental safety. Uranium raw materials enrichment lasted in Ukraine until the Soviet Union fell apart in 1991. Currently, there are about 120 local contaminated sites that are identified inside and near Kamianske (former city name is Dniprodzerzhynsk). The exposure dose of these spots in several times is higher than the control.

Production Association of Pre-Dnieper chemical plant (PA PCP) was one of the most powerful uranium enterprises of the former USSR. Activity of the enterprise has led to formation of uranium ore traces. In particular, they can appear in a form of specific contamination fractions on the surface of the soil. Such focal points of the radiation pollution are enriched with radium-226 and other uranium-thorium radionuclides. They have been formed as a result of uranium extraction and ore recycling. There are nine radioactive waste storage facilities developed since the production at the PA PCP was launched. They are placed at the plant site as well as adjacent areas.

Radioactive solid and liquid waste is accumulated in gullies and hollows and on the upper terrace of the Dnieper river near other mining and metallurgical enterprises. Agricultural lands adjoin uranium tailings from all sides. Each year, as a result of wind erosion, more than 30 tons of radioactive dust settles on the arable lands. Also, radionuclides may be discharged to the atmosphere through by radon emanation.

Production of uranium concentrate was halted on PCP in connection with Soviet Union collapse. Several liquidation-reclamation actions were made within environmental programs to manage safe condition of uranium production with PCP [3, 4]. However, the management and maintenance of these neglected facilities are still problems of the current interest. Therefore, environmental security requires the use of modern technologies [5].

A set of environment security technologies are needed to be implemented to monitor, assess, and visualize the agricultural soil contamination. It will give an ability to prepare for, respond to, and manage potential adverse effects from radioactive pollution.

The goal of the research was the elimination of the negative environmental effects of the PCP activity. Uranium milling activities is a source of considerable soil contamination by radioactive substance, making a harmful impact on environment and the population. Regular radioecological observations and up-to-date contamination mapping become a primary issue for environmental protection of areas surrounding uranium ore milling works. Hyperspectral satellite imagery provides a potentially powerful tool for radioactive pollutant detection and mapping.

http://dx.doi.org/10.5772/intechopen.72601

2. Main sources and ways of soil contamination

2.1. Uranium mill tailings deposits

The Sukhachevske tailings dump and Base S tailings deposit are located on the right bank of the Dnieper 5 km southeast of Kamianske (**Figure 1a**).

The Sukhachevske wet uranium tailings dump is still partly covered with water. The dump is located on the left branch of the Rozsoluvata ravine in the Sukha Sura river valley. The tailings' construction is a ravine partitioned by two dams and consisted of two sections, one arranged behind the other (**Figure 1b**). Base S tailings deposit is located 830 m east of the Sukhachevske tailings dump.

The chemical composition of wastes formed the major source of uranium ore minerals (quartz, feldspar, hydromica, kaolinite) combined with the chemicals used during ore processing (sulfuric and nitric acid) and products of neutralization of the resulting acidic environment (lime). The exposure dose rate of gamma radiation on the surface of the waste not covered by water varies from 100 to 1800 mcR/h. Power of equivalent dose of gamma radiation at a height of 1 m above the surface of the stored materials is changed in the downstream part from 0.31 to 4.08 μSv/h, in the upper reaches of 0.59–4.4 μSv/h, and averages the lower section of 1.91 ± 0.55 μSv/h.

The concentrations of radon-222 in the waste varies from 0.17 ± 0.03 MBq/m^3 to 1.73 ± 0.25 MBq/m^3 at a depth of 0.6 m. The flux density of radon-222 from the surface is in the range of 0.03–1.475 Bq/m^2·s.

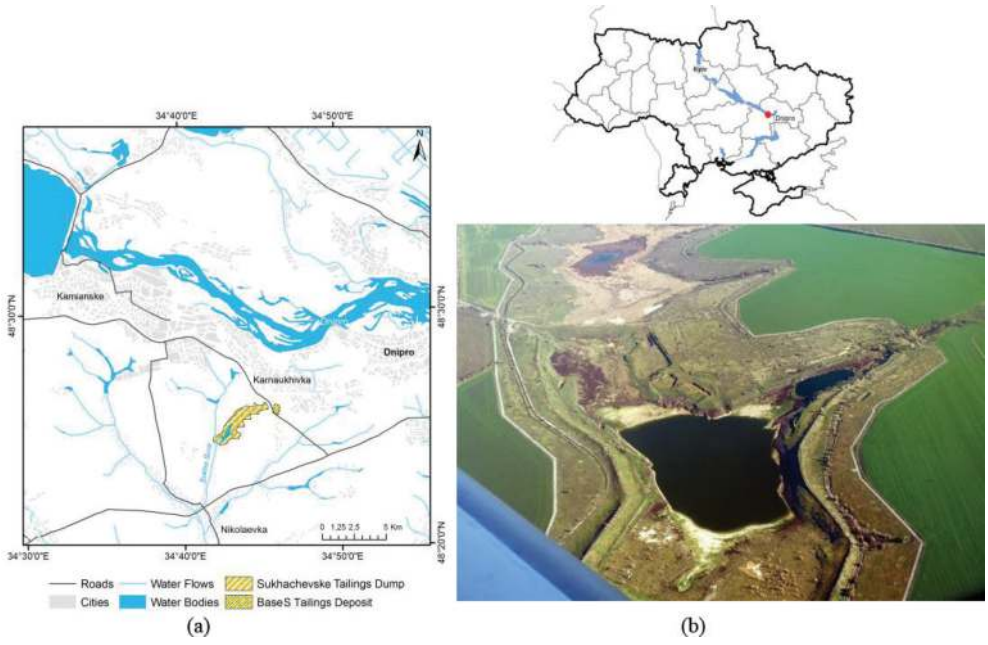

Figure 1. Location of the main uranium mill tailings deposits around Kamianske city (a) and an aerial photo of Sukhachevske tailings dump from http://wikimapia.org (b).

Liquid waste is represented by the waters of a pond in the central part of the tailings dump and pore water in the bulk of the solid waste. The slurry water contains barium, cadmium, strontium, cobalt, fluoride, nickel, zinc, silicium, manganese, and aluminum.

The main purpose of another tailings deposit—Base S—was a temporary warehousing of raw uranium delivered to the plant for further processing. It was built in 1960 and was in operation until 1990.

Now, the technology for waste storage at the tailings dump is disturbed: water pumping stations and conduits were destroyed; the feeding of water to the tailings dump was terminated; fencing facilities are destroyed in many places; and sewage water pipeline from PCP to the Sukhachevske uranium tailings dump suffered from numerous violations and corrosion. As a result, radioactive dust and sewage water have contaminated surrounding areas.

2.2. Ways of radioactive contamination spreading

2.2.1. Wind-driven spread of contaminants

The frequency of repetition directions of the wind is one of the determining factors to assess the transport of fine particles from the surface of waste storage. The right side of Kamianske city is under prevailing southerly wind spreading. This fact coincides with increment of technogenic load from the southern side of the second section of Sukhachevske tailings dump [6]. The predominant annual average wind frequency of occurrence has its maximum in north-northwest direction (**Figure 2**). However, the excess over the rest is minimal.

Average wind speed is in the range of 2.9–4.4 m/s (**Table 1**).

A large part of the surveillance zone near the Sukhachevske tailings dump is used for agricultural production. About 90% of the total area of farmland is plowed and used for cereals (wheat, barley, corn, oats), forages, and technical crops (sunflower and rape) cultivation. Lower slopes and bottoms of the ravines are used for haymaking and grazing. The forest vegetation in the area is represented by forest belts on the plateau and its slopes. Each year, because of wind erosion, considerable amount of contaminated dust particles settle on arable lands.

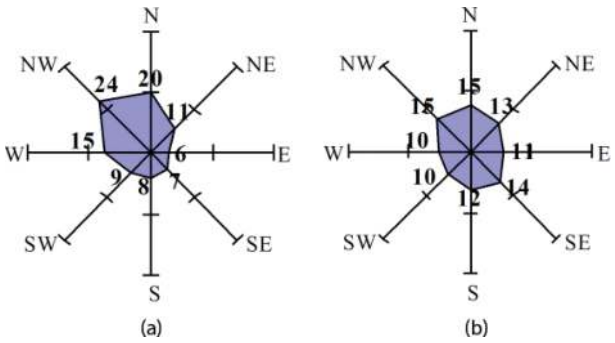

Figure 2. Frequency of wind directions (%) by long-term observations: (a) July average and (b) annual average [7].

Month	I	II	III	IV	V	VI	VII	VIII	IX	X	XI	XII	Year
Wind speed (m/sec)	4.2	4.4	4.2	3.9	3.3	3.2	3.0	2.9	3.0	3.5	3.6	3.8	3.6

Table 1. Average month and annual wind speed by long-term observations (m/s) [7].

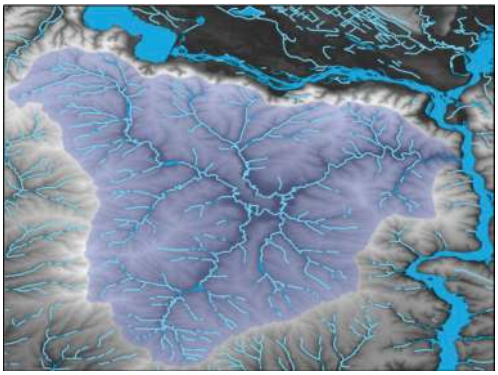

Figure 3. Basin of the Mokra Sura river.

2.2.2. Transfer of contaminants by hydrological network and surface runoff

Surface runoff from contaminated land is one of the major processes responsible for the contamination of water bodies. From the catchment area, the contaminants draining into the streams accumulate in floodplains and riverbeds. Rivers, drying out in warm seasons, cause secondary wind-driven contamination.

The Sukha Sura river is a tributary of the Mokra Sura river. Meantime, the pool of the Mokra Sura river is bordered with pool of the Samotkan river from the northwest, with the river Bazavluk in the southwest, with the Tomakovka river from the east, and near the Dnieper river from the north and east (**Figure 3**).

3. Materials and methods

3.1. Target and background spectral separation

Known algorithms for polluting agents' detection, which are used to analyze the spectrometric measurements, are based on the target and background spectral separation [8]. Therefore, the target spectra are necessary before starting the analysis of hyperspectral imagery. Before hyperspectral imaging engagement, the spectrometric measurements of contaminated soil samples were performed in ground control points (GCP), which are plotted in **Figure 4a**. Soil equivalent dose rate measurements were performed 10 times for each sample and then averaging (**Tables 2** and **3**).

Laboratory spectrometric measurements of field samples were carried out using the FieldSpec 3FR high-precision portable spectrometer (**Figure 4b**) developed by Analytical

Spectral Devices, Inc. (ASD, Inc.) company (http://www.asdi.com//). The main specifications of FieldSpec 3FR instrument are as follows: spectral range is 350–2500 nm, spectral sampling interval is 1.4 nm inside 350–1000 nm range, 2 nm inside 1000–2500 nm range, and output spectral sampling interval is 1 nm (interpolated).

Spectra of the field samples measured using FieldSpec3FR were calibrated as absolute reflectance, including both reflectance value and standard deviation. It is clear that to match the

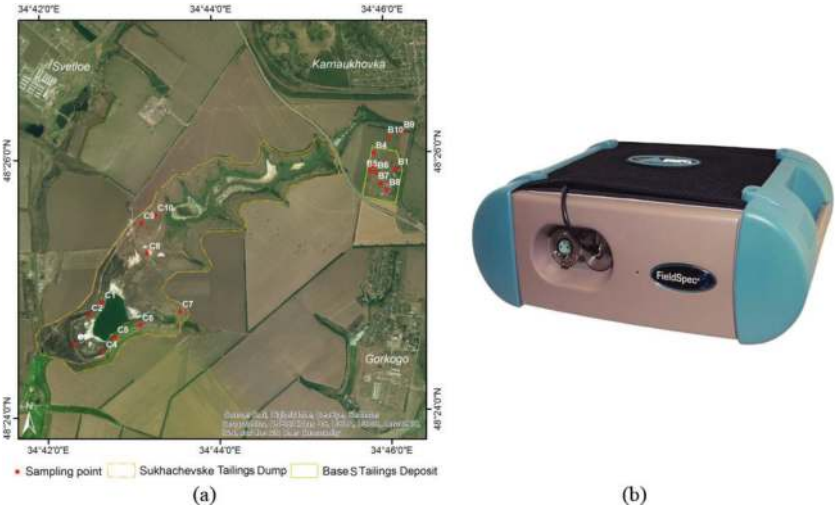

Figure 4. Ground control points of in situ measurements (a) and ASD FieldSpec 3FR portable spectrometer used for spectrometric measurements of contaminated soil samples (b).

	The Sukhachevske tailings dump									
Point code	C 1	C 2	C 3	C 4	C 5	C 6	C 7	C 8	C 9	C 10
Equivalent dose rate (μSv/h)	0.11–0.16	0.10–0.14	0.09–0.12	0.12–0.16	0.11–0.14	0.08–0.12	0.09–0.13	0.69–0.80	0.16–0.19	0.18–0.23

Table 2. Results of in situ measurements of soil equivalent dose rate at the Sukhachevske tailings dump.

	The Base S tailings deposit									
Point code	B 1	B 2	B 3	B 4	B 5	B 6	B 7	B 8	B 9	B 10
Equivalent dose rate (μSv/h)	1.15–1.24	0.38–0.44	0.21–0.26	0.15–0.21	0.39–0.46	0.39–1.08	2.22–2.41	2.02–2.13	0.14–0.18	0.13–0.17

Table 3. Results of in situ measurements of soil equivalent dose rate at the Base S tailings deposit. Comparative to average background within Dniprodzerzhinsk city [7] equivalent dose rate in points B1, B6, B7 and B8 was 8-17 times more.

http://dx.doi.org/10.5772/intechopen.72601

FieldSpec 3FR and Hyperion spectra correctly, the latter one should be recalibrated to land surface reflectance too.

The target spectra of soil samples at sites B and C within PCP acquired by FieldSpec 3FR spectrometer are shown in **Figure 5**.

3.2. Hyperspectral imagery time series and preprocessing

The Hyperion imaging spectrometer was part of the NASA's Earth Observing Mission 1 (EO-1). Hyperion was the first imaging spectrometer to routinely acquire science-grade data from Earth orbit. Its 242 bands covered the visible, near-infrared, and shortwave infrared bands (400–2500 nm) with 10 nm bandwidths. The spatial resolution of 30 m was sufficient to address most land application issues [9].

Images are available for free download through the United States Geological Survey (USGS) EarthExplorer. Timeline includes EO-1/Hyperion products on the 4-year period from 20 July 2012 to 13 July 2016 (**Figure 6**). All the images have been radiometrically calibrated based on *gain* and *offset* values from metadata file. As a result, a stack of 196 bands in 426–2395 nm range for each image have been formed.

The images were converted into surface reflectance using MODTRAN 4 atmospheric model approach [10]. It uses only approximate specification of sensor band locations (i.e., central wavelengths) and their radiometric calibration; no additional metadata were required [11].

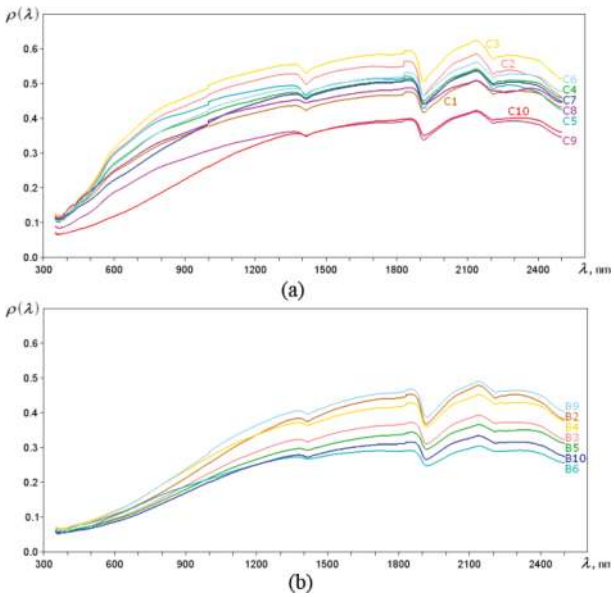

Figure 5. Target spectra of soil samples: (a) at the Sukhachevske tailings dump and (b) at the Base S tailings deposit.

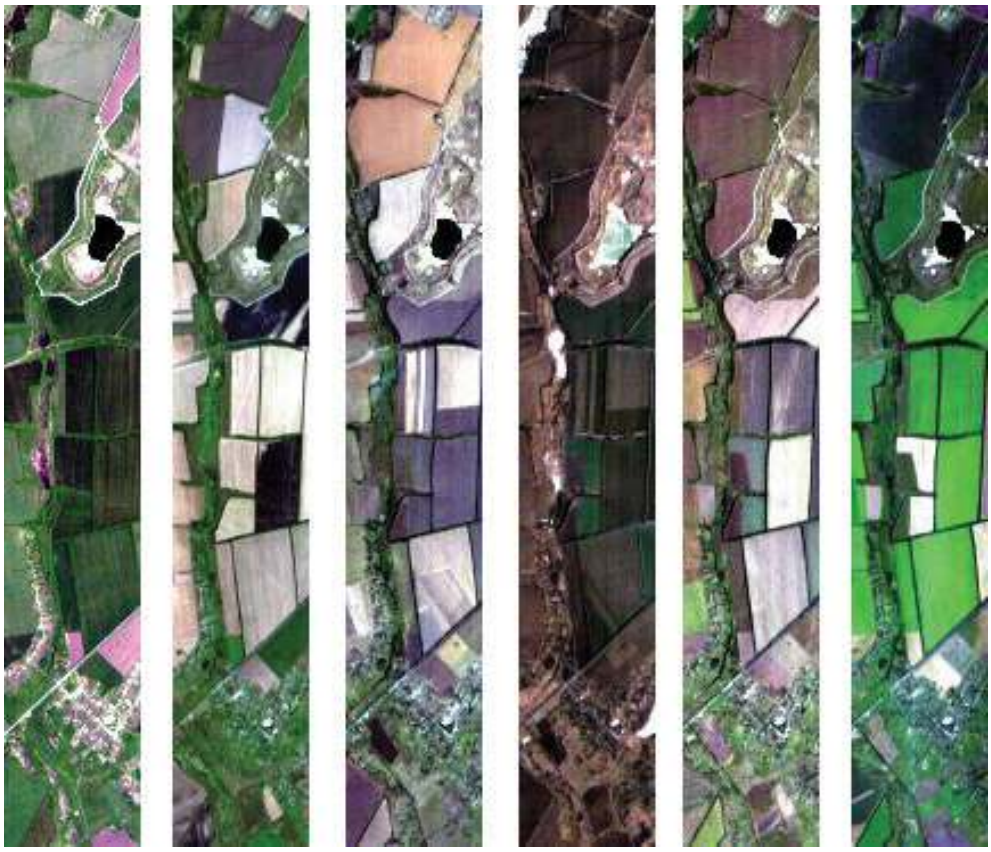

Figure 6. EO-1/Hyperion images over the Sukhachevske tailings dump: Band combinations are *R*, 640; *G*, 548; and *B*, 487 nm.

Each band of every image of timeline was checked on salt-and-pepper noise in two iterations by signal-to-noise ratio (SNR). Bad band list was formed to remove low SNR bands [12]. New stack for images consists of 87 bands in 487–2324 nm range. All the images have been clipped by image coordinate system and geo-referenced.

3.3. Hyperspectral imagery processing for target spectral mapping

Usually, polluting substances are present in the soil in a small amount and therefore contribute insignificantly to the overall reflection spectrum. A spectral unmixing technique is used to detect such small impurities. Coarse spatial resolution of hyperspectral imager leads to the possibility of several different spectra capturing jointly, causing errors in their separation [13]. If the spectral samples are quite a few, it is possible to separate the different spectral one from another, even within a joint field of view. The linear unmixing model is used most commonly. This model calculates the contribution of each spectrum available

http://dx.doi.org/10.5772/intechopen.72601

within the field of view. Linear unmixing model provides the homogeneous spectral weighing in proportion to their fractions within the field of view [14]. Methods and algorithms for spectral unmixing are developed for decades [15]. In our case the hyperspectral imagery from NASA's EO-1/Hyperion satellite sensor (https://eo1.gsfc.nasa.gov/) was used. This instrument operates in 400–2500 nm spectral range with 30 m spatial resolution on the ground surface [16].

The general processing dataflow is described by the flowchart in **Figure 7** diagram.

Both hyperion sensor and FieldSpec spectrometer raw data are calibrated for land surface reflectance output. Then, the high spectral resolution FieldSpec data transformed into Hyperion's spectral signatures through the FieldSpec's spectral convolution with Hyperion's band spectral responses [17]. Now, it is possible to perform pixel-by-pixel matching of the target and current signatures for spectral fraction mapping. The matching procedure implies simultaneous reliability evaluation of the target signature retrieving. Further, these estimates are used to adjust the values of detected target spectral fractions (the fusion operator). Finally, the distribution maps of the target spectra are generated for the entire hyperspectral image scene.

The spectral unmixing model assumes that every ith spectral signature, $i = 1 \ldots n$, can be written as an m-dimensional vector y_i, where m is the number of spectral samples, and each jth target spectrum—by an m-dimensional vector x_j, $j = 1 \ldots p$. Let X as the matrix of target spectra of size $m \times p$, and $\alpha_i = (\alpha_1, \alpha_2 \ldots \alpha_p)^T$ as the vector of target spectral fractions in the ith spectral signature. Linear mixing model for y_i spectrum is expressed by equation:

$$y_i = X\alpha_i + \varepsilon_i \tag{1}$$

where ε_i is the residual vector which can be considered as the additive noise [18].

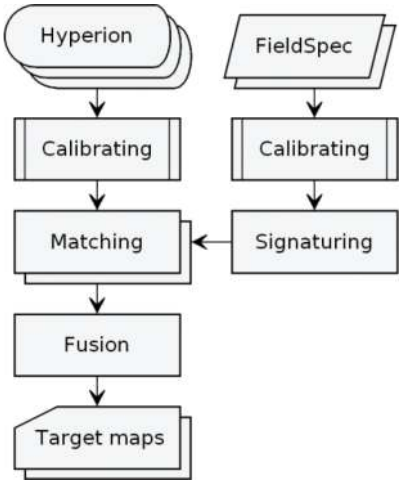

Figure 7. Hyperspectral imagery general flowchart.

The main restriction of unmixing is exceedance of the spectral sample number over the number of target spectra which are unmixed:

$$m \geq p \tag{2}$$

If all elements of X matrix are known, then the problem comes down to solving a system of linear equations by least squares (LS) method, possibly with some constraints: nonnegatively (nonnegatively constrained least squares (NCLS)), sum-to-one equality (sum-to-one constrained least squares (SCLS)), or both simultaneously (fully constrained least squares (FCLS)). In [8] paper a special algorithm based on modified FCLS method was proposed.

Unfortunately, in practice, as a rule, the all spectral composition of the whole scene is unknown. In this case the other method must be applied which extract one or more known target spectra, and the rest are considered as unwanted [19]. The TCMI (target-constrained minimal interference) filter, proposed in [20] paper, is the most perfect of such methods. In TCMI filter the estimation of sum of target spectral fractions in ith signature is equal to $w^{\mathrm{T}} y_i$, where y_i is the mixed spectrum and w is the solution of minimization problem:

$$\begin{cases} \mathrm{w}^{\mathrm{T}} \mathrm{x}_{\mathrm{j}} = \begin{cases} 1 & \text{if j is target} \\ 0 & \text{otherwise} \end{cases} \\ \mathrm{j} = 1 \ .. \ \mathrm{p} \\ \sum\limits_{\mathrm{i}=1}^{\mathrm{n}} \left(\mathrm{w}^{\mathrm{T}} \mathrm{y}_{\mathrm{i}}\right)^2 \rightarrow \min \end{cases} \tag{3}$$

Generally, it is can be assumed that the first k spectra are the target and rest $k + 1 \ldots p$ ones are unwanted. Then, an explicit formula for w will be as follows:

$$w^{\mathrm{T}} = \left(\underbrace{1..1}_{k}, \underbrace{0..0}_{p}\right) (X^{\mathrm{T}} Y^{-1} X)^{-1} X^{\mathrm{T}} Y^{-1} \tag{4}$$

where $Y = \sum\limits_{i=1}^{n} y_i y_i^{\mathrm{T}}$.

If the target signature is alone, then the TCMI filter is simplified to the CEM (constrained energy minimization) one [21]. Thereupon,

$$w_{\mathrm{CEM}}^{\mathrm{T}} = \frac{x_1^{\mathrm{T}} Y^{-1}}{x_1^{\mathrm{T}} Y^{-1} x_1}$$

where x_1 is the target spectrum.

In order to apply the TCMI filter for target spectral fractions, the ones estimations in ith mixed signature will be.

$$\alpha_{\mathrm{TCMI}i} = (X^{\mathrm{T}} Y^{-1} X)^{-1} X^{\mathrm{T}} Y^{-1} y_i \tag{5}$$

where $\alpha_{\mathrm{TCMI}i}$ is a p-dimensional vector. The TCMI and CEM filters can be reduced to linear transform of spectra with the kind of a LS method also known as the OSP (orthogonal subspace projection) method [22].

Any components of α_{TCMIi} vector can be negative. Theoretically, the small value of fraction estimate indicates that this spectrum is not present inside mixed signature. Nevertheless, the negative values are unacceptable as fraction estimates. To avoid the negative values of estimates, it is reasonable to apply a method similar to the NCLS. Such improvement of the classical TCMI algorithm was proposed in [23] paper.

Combination of the TCMI and NCLS methods consists in finding a target spectral fractions α_i in the ith mixed signature as a minimum value in the equation system with constraints:

$$\begin{cases} (y_i - X\alpha_i)^T Y^{-1} (y_i - X\alpha_i) \rightarrow \min \\ \alpha_{ij} \geq 0,\ j = 1,\ 2\ ..\ p \end{cases}$$

Like TCMI and CEM, the TCMI-NCLS method is reduced to spectral multiplication by the $Y^{-1/2}$ matrix and to succeed application of the NCLS method. The TCMI-NCLS algorithm provides a higher accuracy than the classical TCMI in spectral unmixing for land cover classification [23].

The processing of hyperspectral imagery for soil contamination mapping of study area was carried out through the determination of target spectral fractions in each hyperspectral pixel by the TCMI-NCLS algorithm.

Our previous experience has shown that it is necessary to estimate the error probability and to adjust the expected values of target spectral fractions (the Fusion procedure) for reliable results. Similar approach was applied for soil contamination mapping within Kiev city area using the hyperion hyperspectral image [24]. Techniques based on information divergence [25], Bhattacharyya statistical distance [26], spectral-topological classifier [27], and fuzzy decision tree [28] were considered. Finally, the information divergence and Bhattacharyya statistical distance were involved to adjust the target spectral fractions after TCMI-NCLS algorithm applying over input hyperspectral image.

It is possible to ensure further improvement in evaluation reliability by analyzing the time series of research area imagery rather than stand-alone images. Time series analysis is a universal tool for the systems and process state assessment, as well as for its prediction. Time series analysis is especially important for the remote sensing data processing [29]. The purpose of time series analysis is to determine the parameters of the occurring change dynamics, primarily the trend and periodic components [30]. The Earth's surface imagery time series should be considered as composite of individual time series in each pixel.

4. Results and discussion

In the current research, the subfractions of each target spectrum were summed up, and in this way, the maps of spatial distribution of soil with pollution has been formed. **Figure 8** contains the spatial distribution of the total fractions of target spectra within the scene of the study area. Since the applied algorithm detects contaminant fractions only on the surfaces of exposed soil and has restrictions for detecting them on other soils covered with snow or vegetation, spatial distribution of the total fractions of target spectra is differently represented in the images of

certain stages of the season. The least indicative are the images of the warm period when most of the study area is covered by natural (in the floodplain of the Sukha Sura river) or agricultural (on the arable lands) vegetation as it can be seen from the images of 10 May 2013, 20 July 2013, and 13 July 2016. The image for the snowless winter period (18 February 2015) demonstrates spatial distribution of the contaminant fractions most entirely, excepting small areas of artificial surfaces and areas covered with snow and ice. Spatial distributions of the contaminant fractions on the images of the autumn period (18 September 2014, 17 September 2015) are reflected depending on the soil exposure and the way it was cultivated during agricultural works and differ from year to year. Besides, the detection of contaminant fractions can also be affected by the state of the soil at the time of survey, to the extent that it is waterlogged, cultivated, or eroded.

The pixel-by-pixel simultaneous processing of all target spectral maps resulted in spatial distributions of time series parameters. Because the total number of hyperspectral images in time series was not too large, an analysis of their time series turns into the linear trend extracting [31]. The linear trend is described by two independent parameters: the average value for the entire observation period and the daily mean increment. The results of parameter calculation of Hyperion image's time series linear trend for both scenes are illustrated in **Figure 9**.

The data on average value and daily increment show hot spots of high technogenic load around Rozsoluvata ravine.

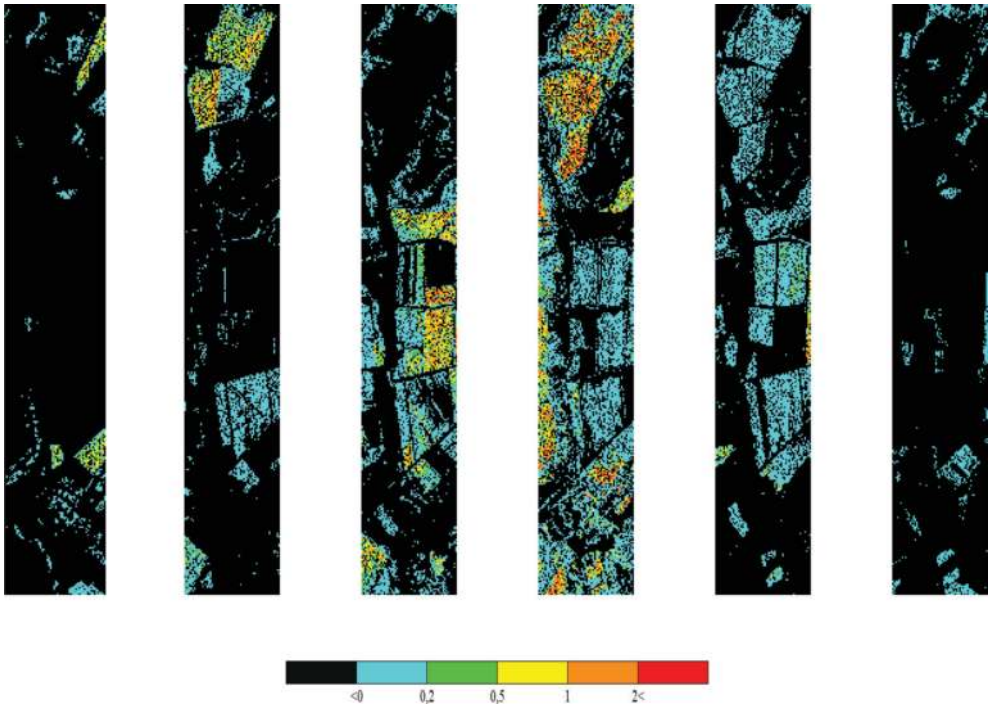

Figure 8. Target spectral total fractions by fused TCMI-NCLS algorithm.

http://dx.doi.org/10.5772/intechopen.72601

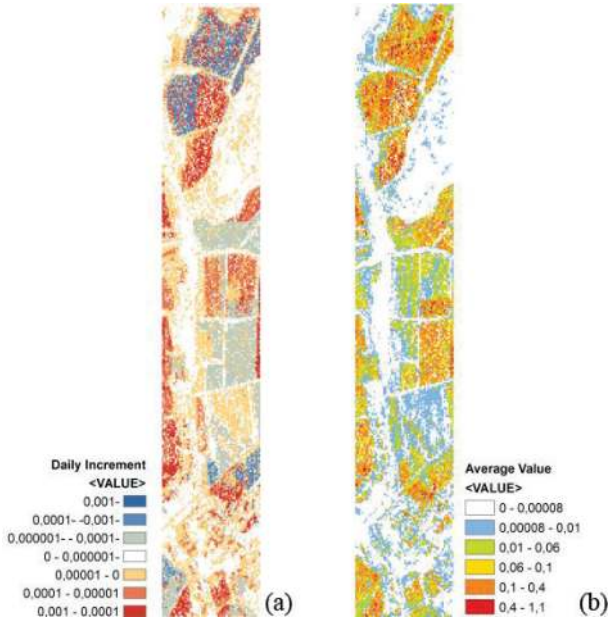

Figure 9. Spatial distributions of the time series parameters: (a) daily mean increment and (b) average value for the entire observation period.

5. Conclusions

Our research was made with intention to find a relation between remotely sensed hyperspectral and ground-based measured soil contamination fractions in the area of the uranium mill tailings deposits. Other types of urban industrial landscapes were not involved in the process of hyperspectral classification. Airborne dust and erosion processes were selected as the main reasons of environment pollution with radionuclides and heavy metals in the territory occupied with two tailings of uranium mill tailings. The spectra of field samples taken near the two deposits were compared with hyperspectral images. The maps on average value and daily increment assessment are background to classify area with different levels of technogenic load.

Additionally, our research has confirmed that hyperspectral imaging is a useful and an efficient tool for soil contamination mapping. One allows to detect small contaminant fractions on the soil surface by spectral end-member unmixing, if it is not shaded by vegetation or other covers. The proposed NCLS-TCMI algorithm is more advanced than the known CEM and TCMI ones, and it provides more reliable detection of soil contaminant's fractions. At the same time, the similarity of contaminated and non-contaminated soils' spectra and the small value of detected fractions have resulted in the need for additional adjustment of mapping outputs. This specified problem can be mitigated by taking certain measures when preparing the input data and carrying out the mapping. First, the reference spectra should be prepared

not only for soils but also for other land covers within the scene. This will make it possible to carry out a full-scale land cover classification and to build a mask of soil of interest only before the final mapping. Second, the reference spectra of both contaminated and non-contaminated soils are required for contaminants' reliable detection. This will permit the Bayesian rule engagement for similar spectral discrimination.

Future works should be devoted to the development of complete all-in-one technology for mapping of soil contamination using hyperspectral imagery and its wide-ranging statistically significant probation over variety of test sites.

Author details

Sergey A. Stankevich[1]*, Mykola M. Kharytonov[2], Anna A. Kozlova[1], Vadym Yu. Korovin[3], Mykhailo O. Svidenyuk[1] and Alexander M. Valyaev[3]

*Address all correspondence to: st@casre.kiev.ua

1 Scientific Centre for Aerospace Research of the Earth, NAS of Ukraine, Kiev, Ukraine

2 Dnepropetrovsk State Agrarian and Economy University, Dnipro, Ukraine

3 Institute of Geotechnical Mechanics, NAS of Ukraine, Dnipro, Ukraine

References

[1] Kharytonov MM, Pashova VT, Bagorka MO, Kozechko VI, Dudar TO. Arable lands degradation in the northern steppe zone of Ukraine. Agriculture and Forestry. 2016;**62**(2):71-80. DOI: 10.17707/AgricultForest.62.2.05

[2] Kharytonov M, Bagorka M, Gibson P. Erosion effects in the central steppe chernozem soils of Ukraine. I. Soil properties. Agricultura [Internet]. 2004;**3**(1):12-18. ISSN 1581-5439. Available from: http://www.agriculturaonline.com/portal [Accessed: October 18, 2017]

[3] Voigt G, Fesenko S, editors. Remediation of contaminated environments. In: Baxter MS, editor. Radioactivity in the Environment. 1st ed. Amsterdam: Elsevier Science; 2009. 14. 496 p. ISBN: 978-0-08-044862-6

[4] Smičiklas I, Šljivić-Ivanović M. Radioactive contamination of the soil: Assessments of pollutants mobility with implication to remediation strategies. In: Marcelo LL, Sonia S, editors. Soil Contamination – Current Consequences and Further Solutions. Rijeka: InTech [Internet]; 2016. pp. 253-276. DOI:10.5772/64735. Available from: https://www.intechopen.com/books[Accessed: October 18, 2017]

[5] Stankevich SA, Kharytonov NN, Dudar TV, Kozlova AA. Risk assessment of land degradation using satellite imagery and geospatial modelling in Ukraine. In: Kaswamila A, editor. Land Degradation and Desertification – A Global Crisis. Rijeka: InTech; 2016. pp. 53-77. DOI: 10.5772/61629

[6] Kharytonov M, Benselhoub L, Shupranova A, Kryvakovska R, Khlopova V. Environmental assessment of atmospheric pollution in Dnipropetrovsk province (Ukraine). Studia Universitatis "Vasile Goldis". 2015;**25**(2):125-130. ISSN: 1584-2363

[7] Environmental passport of Dneprodzerzhinsk city. Dnepropetrovsk; 2003. p. 144

[8] Stankevich S. Land-cover classification on hyperspectral aerospace images by spectral end members unmixing. Journal of Automation and Information Sciences. 2006;**38**(12):31-41. DOI: 10.1615/J Automat Inf Scien.v38.i12.40

[9] Pearlman J, Barry PS, Segal CC, Shepanski J, Beiso D, Carman SL. Hyperion, a space borne imaging spectrometer. IEEE Transactions on Geoscience and Remote Sensing. 2003;**41**(6):1160-1173. DOI: 10.1109/TGRS.2003.815018

[10] San BT, Suzen ML. Evaluation of different atmospheric correction algorithms for EO-1 Hyperion imagery. International Archives of the Photogrammetry, Remote Sensing and Spatial Information Science. 2010; **XXXVIII**(8):392-397. EID: 2-s2.0-84877874959. Available from: http://www.isprs.org/proceedings/XXXVIII/part8/pdf/W03C05_20100306205904.pdf [Accessed: October 28, 2017]

[11] Bernstein L, Jin X, Gregor B, Adler-Golden S. Quick atmospheric correction code: Algorithm description and recent upgrades. SPIE Optical Engineering. 2012;**51**(11):111719-1-111719-11. DOI: 10.1117/1.OE.51.11.111719

[12] Lukin V, Ponomarenko N, Fevralev D, Vozel B, Chehdi K, Kurekin A. Classification of pre-filtered multichannel remote sensing images. In: Escalante-Ramirez B, editor. Remote Sensing – Advanced Techniques and Platforms. Rijeka: InTech Open; 2012. p. 75-98. DOI:10.5772/1808. Available from: https://www.intechopen.com/books[Accessed: October 28, 2017]

[13] Melesse AM, Weng Q, Thenkabail PS, Senay GB. Remote sensing sensors and applications in environmental resources mapping and modeling. Sensors. 2007;**7**(12):3209-3241. DOI: 10.3390/s7123209

[14] Nielsen AA. Spectral mixture analysis: Linear and semi-parametric full and iterated partial unmixing in multi- and hyperspectral image data. International Journal of Computer Vision. 2001;**42**(1-2):17-37. DOI: 0.1023/A:1011181216297

[15] Eismann MT, Hardie RC. Stochastic spectral unmixing with enhanced endmember class separation. Applied Optics. 2004;**43**(36):6596-6608. DOI: 10.1364/AO.43.006596

[16] Ungar SG, Pearlman JS, Mendenhall JA, Reuter D. Overview of the earth observing one (EO-1) mission. IEEE Transactions on Geoscience and Remote Sensing. 2003;**41**(6):1149-1159. DOI: 10.1109/TGRS.2003.815898

[17] Cundill SL, van der Werff HMA, van der Meijde M. Adjusting spectral indices for spectral response function differences of very high spatial resolution sensors simulated from field spectra. Sensors. 2015;**15**(3):6221-6240. DOI: 10.3390/s150306221

[18] Popov MA, Stankevich SA, Moldovan VD. Artificial objects detection by subpixel processing of hyperspectral aerospace imagery (Ukrainian). Journal of State Aviation Research Institute Kyiv; December. 2006;**9**(2):194-204

[19] Chang C-I. Hyperspectral Imaging: Techniques for Spectral Detection and Classification. N.Y: Kluwer Academic/Plenum Publishers; 2003. p. 396. DOI: 10.1007/978-1-4419-9170-6

[20] Kwan C, Ayhan B, Chen G, Wang J, Ji B, Chang C-I. A novel approach for spectral unmixing, classification, and concentration estimation of chemical and biological agents. IEEE Transaction on Geoscience and Remote Sensing. 2006;**44**(2):409-419. DOI: 10.1109/TGRS.2005.860985

[21] Farrand WH, Harsanyi JC. Mapping the distribution of mine tailings in the Coeur d'Alene River valley, Idaho, through the use of a constrained energy minimization technique. Remote Sensing of Environment. 1997;**59**(1):64-76. DOI: 10.1016/S0034-4257(96)00080-6

[22] Harsanyi JC, Chang C-I. Hyperspectral image classification and dimensionality reduction: An orthogonal subspace projection approach. IEEE Transactions on Geoscience and Remote Sensing. 1994;**32**(4):779-785. DOI: 10.1109/36.298007

[23] Stankevich SA, Shklyar SV. Advanced algorithm for endmembers unmixing on hyperspectral image (Ukrainian). In: Proceedings of the 1st Ukrainian Conference with International Participation; May 2008. Kyiv: Naukova Dumka; 2008. pp. 85-89

[24] Popov MA, Stankevich SA, Lischenko LP, Lukin VV, Ponomarenko NN. Processing of hyperspectral imagery for contamination detection in urban areas. In: Alpas H, Berkowicz SM, Ermakova IV, editors. Spinger. Environmental Security and Ecoterrorism. 2011. pp. 147-156. DOI: 10.1007/978-94-007-1235-5

[25] Cover TM, Thomas JA. Elements of Information Theory. New York: Wiley; 1991. 576 p. ISBN 0-471-20061-1

[26] Fukunaga K. Introduction to Statistical Pattern Recognition. San Diego: Academic Press; 1990. 616 p. ISBN 0-12-269851-7

[27] Stankevich SA. Algorithm for statistical classification of remote sensing objects by their spectral-topological features (Ukrainian). In: Proceedings of Scientific Bulletin of National Mining University. Dnepropetrovsk. 2006. 7. pp. 38-40. ISSN 2071-2227

[28] Stankevich SA, Levashenko VG, Zaitseva EN. Multispectral satellite imagery classification using fuzzy decision tree. Communications. Žilina, Slovakia: University of Žilina. 2014;**16**(1):109-113. ISSN: 1335-4205

[29] Hostert P, Griffiths P, van der Linden S, Pflugmacher D. Time series analyses in a new era of optical satellite data. In: Status Quo and the Pathway Ahead. Kuenzer C, Dech S, Wagner W, editors. Remote Sensing Time Series Revealing Land Surface Dynamics: Cham. Springer, Cham; 2015. 22. pp. 24-42. DOI: 10.1007/978-3-319-15967-6_1

[30] Yaffee R, McGee M. An Introduction to Time Series Analysis and Forecasting. 1st ed. San Diego: Academic Press; 2000. p. 528

[31] Verbesselt J, Hyndman R, Newnham G, Culvenor D. Detecting trend and seasonal changes in satellite image time series. Remote Sensing of Environment. 2010;**114**(8):106-115. DOI: 10.1016/j.rse.2009.08.014